Validation of surface velocity estimated from satellite images

Etienne Huot, Isabelle Herlin, Nicolas Mercier, Gennady K. Korotaev, Evgeny Plotnikov

INRIA

INSTITUT NATIONAL DE RECHERCHE EN INFORMATIQUE ET EN AUTOMATIQUE

Validation of surface velocity estimated from satellite images

Etienne Huot, Isabelle Herlin, Nicolas Mercier,

Gennady Korotaev, Evgeny Plotnikov

N° 7658

July, 2011

Observation and Modeling for Environmental Sciences

ISSN 0249-6399 ISRN INRIA/RR--7658--FR+ENG

INSTITUT NATIONAL
DE RECHERCHE
EN INFORMATIQUE
ET EN AUTOMATIQUE

INRIA

centre de recherche
PARIS - ROCQUENCOURT

Validation of surface velocity estimated from satellite images

Etienne Huot, Isabelle Herlin, Nicolas Mercier,
Gennady Korotaev, Evgeny Plotnikov

Theme : Observation and Modeling for Environmental Sciences
Équipe-Projet Clime

Rapport de recherche n° 7658 — July, 2011 — 14 pages

Abstract: This report concerns the validation of surface velocity estimated from satellite images. The estimation is obtained with a dynamic model based on shallow-water equations. We first compare the stationary assumption to the shallow-water heuristics to justify our choice. Second, we quantify the quality of the estimation by measuring the misfit between the model output and the altimetry measures. Experiments are achieved on Sea Surface Temperature data acquired by the NOAA/AVHRR satellites over the Black Sea. The altimetry measures are obtained by two radar sensors: Envisat and GFO. The good adequacy between the shallow-water output and the altimetry data validates our motion estimation approach.

Key-words: data assimilation, motion estimation, shallow-water

Centre de recherche INRIA Paris – Rocquencourt
Domaine de Voluceau, Rocquencourt, BP 105, 78153 Le Chesnay Cedex
Téléphone : +33 1 39 63 55 11 — Télécopie : +33 1 39 63 53 30

Validation de la vitesse de surface estimée à partir d'images satellites

Résumé : Ce rapport de recherche concerne la validation de l'estimation de la vitesse de surface à partir d'images satellite. Cette estimation est effectuée avec un modèle de la dynamique, basé sur les équations *shallow-water*. Nous comparons d'abord l'hypothèse de stationnarité aux équations *shallow-water* afin de justifier notre choix. Puis, nous quantifions la qualité des estimations en mesurant l'écart entre la sortie du modèle et les mesures d'altimétrie. Les expérimentations sont effectuées en utilisant des données de température de surface, acquises au-dessus de la Mer Noire avec les satellites NOAA/AVHRR. Les mesures altimétriques proviennent de deux capteurs radar : Envisat et GFO. La bonne adéquation entre la sortie du modèle *shallow-water* et les données altimétriques valide notre approche d'estimation du mouvement.

Mots-clés : assimilation de données, estimation du mouvement, shallow-water

1 Introduction

The issue of surface velocity estimation from satellite images has been extensively studied in the literature [1, 2, 3, 4, 5, 6, 7]. Data Assimilation (DA) techniques have been applied in the last five years and gain importance in the scientific community [8, 9, 10, 11]. The key points of the DA approach are: availability of heuristics on the dynamics of a satellite sequence, knowledge on links between velocity and image data.

This paper proposes an analysis and a validation of the DA approach for motion estimation from ocean satellite images. Two *Image Models* were proposed in [12, 13, 14]. They express heuristics on the dynamic of the motion field. The comparison of the estimation using the two models allows us to analyze the impact of these heuristics. The main issue of the paper is then to validate the estimation approach by evaluating the quality of the result, compared to real data.

The motion estimation is performed with NOAA/AVHRR Sea Surface Temperature (SST) data acquired over the Black Sea. The analysis is conducted by comparing the stationary and the shallow-water heuristics. The validation is obtained by quantifying the discrepancy of the water layer thickness, estimated with the shallow-water image model, and the one computed from altimetry data. The altimetry measures, used in this study, come from the Envisat and GFO sensors.

The paper is organized as follows. Section 2 summarizes the principles of variational data assimilation. The definition of the *Stationary Image Model* (SIM) and *Shallow Water Image Model* (SWIM) is given in Section 3. Section 4 describes the application of DA to perform motion estimation. Section 5 describes the SST images (5.1), displays and analyzes the estimated motion result (5.2), describes the altimetry data (5.3), and validates the approach (5.4).

2 Variational Data Assimilation

2.1 Mathematical setting

Let $\mathbf{X}$ being the state vector depending on the spatial coordinate $\mathbf{x}$ ($\mathbf{x} = (x, y)$ for image data) and time t. $\mathbf{X}$ is defined on $A = \Omega \times [0, \tau]$, Ω being the bounded spatial domain and $[0, \tau]$ the temporal domain.

We assume $\mathbf{X}$ is evolving in time according to:

$$\frac{\partial \mathbf{X}}{\partial t}(\mathbf{x}, t) + \mathbb{M}(\mathbf{X})(\mathbf{x}, t) = 0 \tag{1}$$

$\mathbb{M}$, named the *evolution model*, is supposed differentiable.

Observations $\mathbf{Y}(\mathbf{x}, t)$, for instance satellite image acquisitions, are available at location $\mathbf{x}$ and date t and linked to the state vector through an observation equation:

$$\mathbf{Y}(\mathbf{x}, t) = \mathbb{H}(\mathbf{X})(\mathbf{x}, t) + \mathcal{E}_O(\mathbf{x}, t) \tag{2}$$

In this paper, we assume that one component of $\mathbf{X}$ is directly comparable to $\mathbf{Y}$. Consequently, $\mathbb{H}$ reduces to a projection operator. The *observation error* $\mathcal{E}_O$ simultaneously represents the imperfection of the observation operator $\mathbb{H}$ and the measurement errors.

We consider having some knowledge on the initial condition of the state vector at $t = 0$:

$$\mathbf{X}(\mathbf{x}, 0) = \mathbf{X}_b(\mathbf{x}) + \mathcal{E}_b(\mathbf{x}) \tag{3}$$

$\mathbf{X}_b$ is named *background value* of the initial condition and $\mathcal{E}_b$ the *background error*.

$\mathcal{E}_b$ and $\mathcal{E}_O$ are assumed to be Gaussian and fully characterized by their covariance matrices $\mathbf{B}$ and $\mathbf{R}$.

2.2 Variational formulation

In order to solve the system (1), (2), (3) with respect to $\mathbf{X}$ having a maximal *a posteriori* probability given the observations, a functional $E(\mathbf{X})$ is defined and minimized:

$$\begin{aligned} E(\mathbf{X}) = & \int_A [\mathbf{Y}(\mathbf{x},t) - \mathbb{H}(\mathbf{X})(\mathbf{x},t)]^T \mathbf{R}^{-1}(\mathbf{x},t)[\mathbf{Y}(\mathbf{x},t) - \mathbb{H}(\mathbf{X})(\mathbf{x},t)])d\mathbf{x}dt \\ & + \int_\Omega [\mathbf{X}(\mathbf{x},0) - \mathbf{X}_b(\mathbf{x})]^T \mathbf{B}^{-1}(\mathbf{x})[\mathbf{X}(\mathbf{x},0) - \mathbf{X}_b(\mathbf{x})]d\mathbf{x} \\ & + Reg \end{aligned} \tag{4}$$

In this formulation, we consider no correlation of the errors between two space-time positions. *Reg* is a regularization term used to obtain a convex function and allow the minimization process to converge to a global minimum. The minimization of $E(\mathbf{X})$ is carried out with an iterative method based on the one described in [10] and summarized in the following.

At each iteration k, the analysis $\mathbf{X}_a^k$ is obtained from the background $\mathbf{X}_b^k$ by computing the increment $\delta\mathbf{X}$ at $t = 0$.

$$\mathbf{X}_a^k(\mathbf{x}, 0) = \mathbf{X}_b^k(\mathbf{x}, 0) + \delta\mathbf{X}(\mathbf{x}) \tag{5}$$

1. **Initialization**
   (a) $k = 0$
   (b) Compute $\mathbf{X}_b^0(\mathbf{x}, t)$ from the initial condition $\mathbf{X}_b(\mathbf{x})$ of the state vector at $t = 0$ in (3):

$$\mathbf{X}_b^0(\mathbf{x}, 0) = \mathbf{X}_b(\mathbf{x}) \tag{6}$$

$$\frac{\partial \mathbf{X}_b^0}{\partial t}(\mathbf{x}, t) + \mathbb{M}(\mathbf{X}_b^0)(\mathbf{x}, t) = 0, \text{ for } t = 0 \text{ to } \tau \tag{7}$$

   (c) Initialize the analysis $\mathbf{X}_a^0(\mathbf{x}, t)$:

$$\mathbf{X}_a^0(\mathbf{x}, t) = \mathbf{X}_b^0(\mathbf{x}, t) \ \forall t \in [0, \tau] \tag{8}$$

2. **Repeat**
   (a) Compute the adjoint variable λ from $t = \tau$ to $t = 0$:

$$\lambda(\mathbf{x}, \tau) = 0 \tag{9}$$

$$-\frac{\partial \lambda}{\partial t}(t) + \left(\frac{\partial \mathbb{M}}{\partial \mathbf{X}}\right)^* \lambda(t) = \mathbb{H}^T \mathbf{R}^{-1}[\mathbf{Y}(t) - \mathbb{H}\mathbf{X}_a^k], \text{ for } t = \tau \text{ to } 0 \tag{10}$$

(b) Update the value of the background variable:

$$\mathbf{X}_b^{k+1} = \mathbf{X}_a^k \tag{11}$$

(c) Compute the incremental variable $\delta\mathbf{X}$ at $t = 0$:

$$\delta\mathbf{X}(\mathbf{x}) = \mathbf{B}(\mathbf{x})\lambda(\mathbf{x}, 0) \tag{12}$$

(d) Update the value of the analysis variable:

$$\mathbf{X}_a^{k+1}(\mathbf{x}, 0) = \mathbf{X}_b^{k+1}(\mathbf{x}, 0) + \delta\mathbf{X}(\mathbf{x}) \tag{13}$$

(e) Compute $\mathbf{X}_a^{k+1}(\mathbf{x}, t)$ from the initial condition:

$$\frac{\partial \mathbf{X}_a^{k+1}}{\partial t}(\mathbf{x}, t) + \mathbb{M}(\mathbf{X}_a^{k+1})(\mathbf{x}, t) = 0, \text{ for } t = 0 \text{ to } \tau \tag{14}$$

(f) $k = k + 1$

Until $||\delta\mathbf{X}||^2 \leq \varepsilon$

3. Final result is $\mathbf{X}_a^k$.

Equation (10) makes use of the adjoint model $\left(\frac{\partial \mathbb{M}}{\partial \mathbf{X}}\right)^*$. In our study, the discrete adjoint model is automatically obtained by the Tapenade software[1].

3 Image models

The two *Image Models* used in the paper are based on the assumption that a pixel value is a passive tracer transported by the surface velocity field. The state vector $\mathbf{X}$ includes the motion vector $\mathbf{W}$ and a tracer q that can be directly compared to the image observations. The evolution of q is given by the advection-diffusion equation:

$$\frac{\partial q}{\partial t} + \mathbf{W} \cdot \nabla q = \nu_q \Delta q \tag{15}$$

with ν_q standing for the diffusion coefficient.

The *Stationary Image Model* (SIM) is based on the restrictive assumption that, at each position, the velocity is constant over time. The underlying hypothesis is that the surface velocity field evolves much slower than the temperature field. This heuristic is acceptable for a large range of marine processes. If a vortex, whose spatial scale is more than $10 - 50km$, is transported with a velocity less than 0.1 to $0.5m/s$, then the temporal scale of that phenomenon will be more than one day. It means that the surface velocity field can be considered as stationary during one day. Defining $\mathbf{X} = (u, v, q)^T$, with u and v the two components of the 2D motion vector $\mathbf{W}$, SIM is defined as:

$$\begin{cases} \dfrac{\partial u}{\partial t} = 0 \\ \dfrac{\partial v}{\partial t} = 0 \\ \dfrac{\partial q}{\partial t} = -u\dfrac{\partial q}{\partial x} - v\dfrac{\partial q}{\partial y} + \nu_q \Delta q \end{cases} \tag{16}$$

[1] http://www-sop.inria.fr/tropics/

However, the stationary hypothesis makes this image model only applicable on a short temporal window.

The shallow-water equations, derived from the Navier-Stokes equations, link the 2D velocity (u, v) of the layer to its thickness h and take into account the gravity and Coriolis forces. The state vector $\mathbf{X}$ is $(u, v, h, q)^T$ and the *Shallow Water Image Model* (SWIM) is defined as:

$$\begin{cases} \dfrac{\partial u}{\partial t} = -\dfrac{\partial B}{\partial x} + v(f+\xi) + \nu\Delta u \\ \dfrac{\partial v}{\partial t} = -\dfrac{\partial B}{\partial y} - u(f+\xi) + \nu\Delta v \\ \dfrac{\partial h}{\partial t} = -\dfrac{\partial hu}{\partial x} - \dfrac{\partial hv}{\partial y} \\ \dfrac{\partial q}{\partial t} = -u\dfrac{\partial q}{\partial x} - v\dfrac{\partial q}{\partial y} + \nu_q\Delta q \end{cases} \tag{17}$$

with $B = gh + \frac{1}{2}(u^2 + v^2)$, g the reduced gravity, f the Coriolis parameter (depending on the latitude), ξ the vorticity ($\xi = \dfrac{\partial v}{\partial x} - \dfrac{\partial u}{\partial y}$).

4 Application of Data Assimilation

Data Assimilation is applied to perform motion estimation. The sequence of SST images $T(\mathbf{x}, t)$ is assimilated in the two models SIM or SWIM, using the incremental method described in Section 2.2.

As said in Section 2.1, the pixel value $T(\mathbf{x}, t)$ is directly comparable to the component $q(\mathbf{x}, t)$ of the state vector. The observation operator $\mathbb{H}$ reduces to a projection operator, $\mathbb{H}(\mathbf{X}(\mathbf{x}, t)) = q(\mathbf{x}, t)$. The regularization term is based on the L^2-norm of the motion gradient (to obtain a smooth vector field) and on the motion divergency (incompressibilty assumption). Its impact is analyzed in [14]. As we consider perfect models, the value of $\mathbf{X}(t)$ is obtained from the initial conditions $\mathbf{X}(0)$ by integrating in time. Hence, the cost function (4) only depends on the initial conditions and is rewritten as:

$$\begin{aligned} E(\mathbf{X}(0)) = &\int_A (T-q)^T \mathbf{R}^{-1}(\mathbf{x},t)(T-q)d\mathbf{x}dt \\ &+ \int_\Omega \big(\mathbf{X}(0) - \mathbf{X}_b\big)^T \mathbf{B}^{-1}(\mathbf{x})\big(\mathbf{X}(0) - \mathbf{X}_b\big)d\mathbf{x} \\ &\int_\Omega \alpha(|\nabla u|^2 + |\nabla v|^2)d\mathbf{x} + \int_\Omega \beta|div\,\mathbf{v}|^2 d\mathbf{x} \end{aligned} \tag{18}$$

The choice of the covariance matrix $\mathbf{R}$ is crucial for the quality of results. As the satellite images are provided with meta-data information (see section 5.1), the quality of the acquisitions is approximately known. $\mathbf{R}^{-1}(\mathbf{x}, t)$ is then given a small value when the acquisition is noisy at $(\mathbf{x}, t)$ (because of cloud occlusion for instance). The choice of the initial background conditions has also a strong impact on the quality of the result. It has been discussed in [14] that the best results are obtained with the first observation as background for q, null value for $\mathbf{W}$ and a constant value h_m for h, with h_m being the thickness value at rest state. As the background value of q is reliable, $\mathbf{B}_q$ is given a small value.

5 Results

5.1 Image data

A huge amount of images are acquired over the ocean by space remote sensors. Those obtained by optical instruments, such as *Sea Surface Temperature* (SST) data, display a high space-time coherence. The images, used in the paper, are acquired on-board NOAA-AVHRR satellites. Their spatial resolution is 1.1 km^2 at nadir and the temporal revisit is at best one day. However, several acquisitions over the same area are usually acquired on the same day by different satellites. Some of these data are contaminated by clouds or corrupted by noise. Figure 1 displays a SST image acquired over the Black Sea in October 2005, with the cyan color corresponding to clouds or noise.

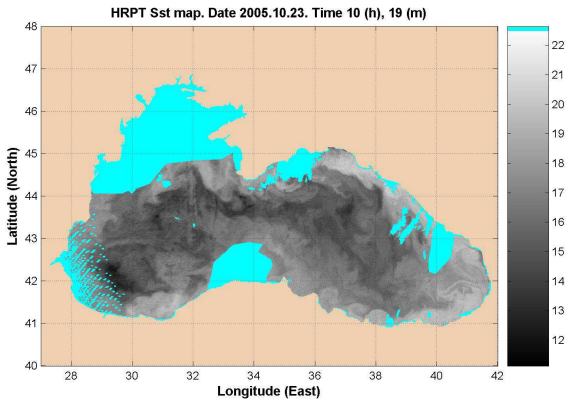

Figure 1: Cyan area corresponds to clouds or noise.

5.2 Analysis

In this paper, motion estimation is tested on a sequence of four images, displayed on Figure 2. The cyan areas, on the third and fourth frames, correspond to missing data.

The two *Image Models* are used to estimate the surface velocity on these data. Figure 3 compares the motion fields estimated with SIM and SWIM, at $t = 0$. The results obtained with SWIM visualize a cyclonic vortex on the western part of the Black Sea. SWIM, due to its physical assumptions on the dynamic, permits a more realistic motion estimation and characterizes structures occuring on the sea surface. In comparison, the potential of SIM highly depends on the size of the temporal window compared to the dynamics involved during that period. That makes SIM no more relevant for data such as those displayed in Figure 2. In conclusion, the DA approach for motion estimation permits to retrieve the major currents of the Black Sea basin. Moreover, the high resolution of NOAA/AVHRR images allows to better evaluate the size of some well known mesoscale structures [12].

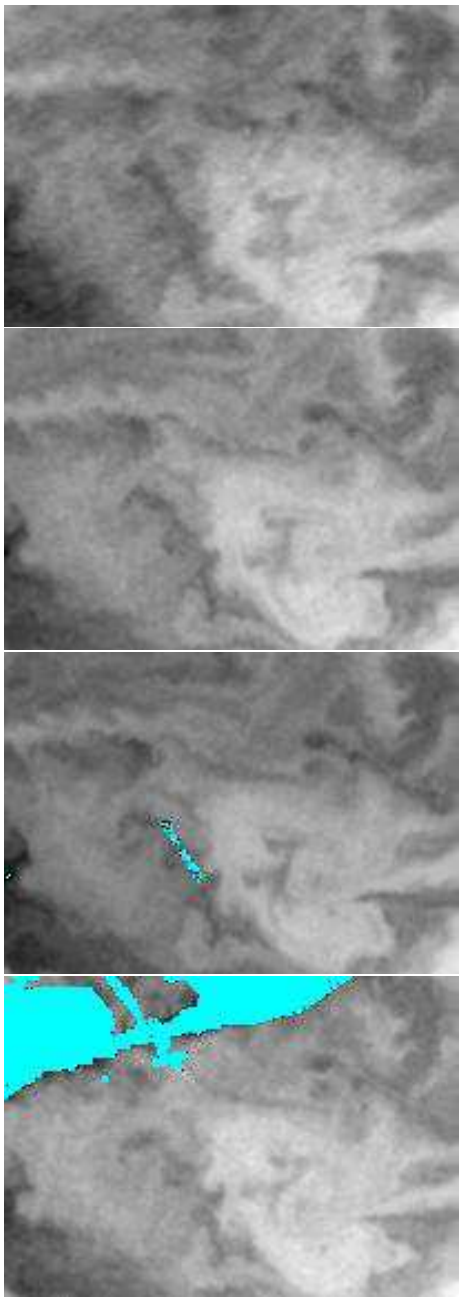

Figure 2: SST data acquired from October 23th to October 24th, 2005.

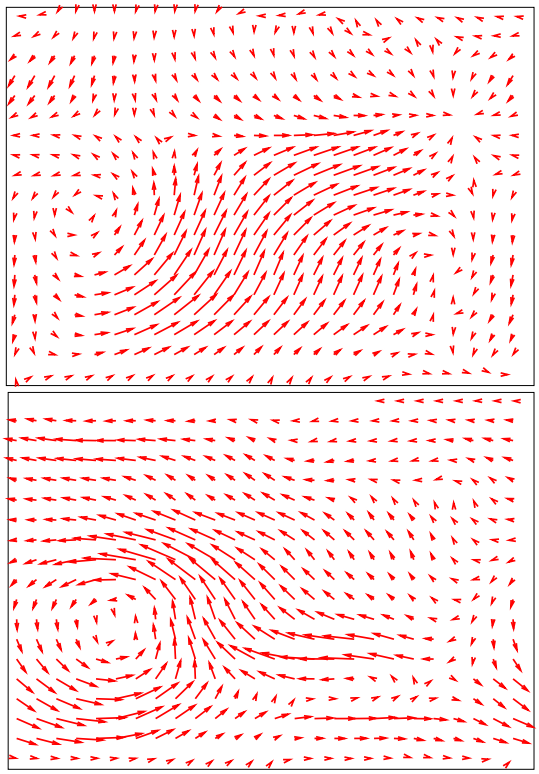

Figure 3: Motion estimation. Up: SIM; down: SWIM.

5.3 Altimetry data

Satellite altimeters provide an accurate measure of the Sea Level Anomaly (SLA) that corresponds to the sea surface deviation from its rest state (see the black curve on Figure 4).

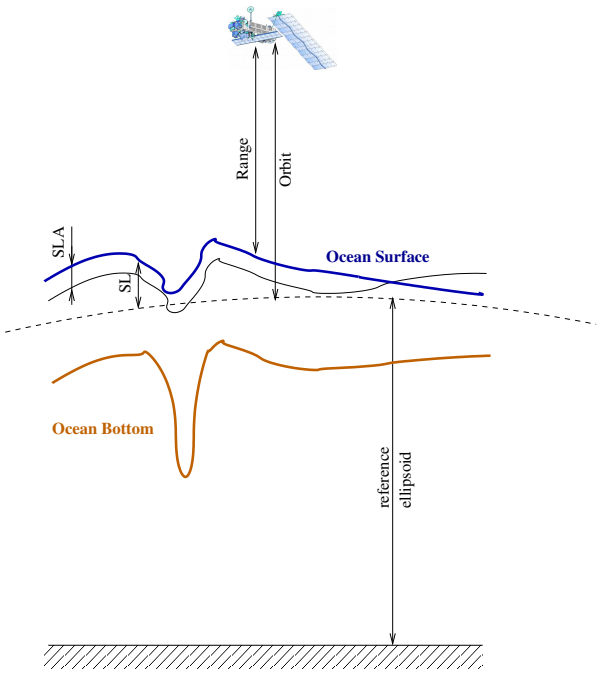

Figure 4: Sea Level Anomaly.

The altimeters are nadir-pointing instruments providing an along-track acquisition. The coverage of Envisat1 over the Black Sea is for instance displayed on Figure 5. In this paper, we use altimetry measures provided by Envisat[2] with a 35 days cycle and by GFO [3] with a 17 days cycle.

5.4 Validation

The outputs of SWIM are $\mathbf{W}$, the surface velocity, and h the thickness of the surface layer. The thickness anomaly, denoted h_{SWIM}, is estimated from h as its deviation from the value at rest. On another hand, the altimeters are 1-dimensional instruments measuring the Sea Level Anomaly, denoted h_{alt}, along their tracks. We then compare h_{SWIM} and h_{alt} at the same positions. The physical formula linking these two quantities is:

$$\rho \times h_{alt} = \Delta\rho \times h_{SWIM} \tag{19}$$

with ρ being the density of the upper layer, $\Delta\rho$ the difference of density between the upper and the lower layer, h_{alt} the sea level anomaly measured by the satellite, h_{SWIM} the thickness anomaly $(h - h_m)$ of the shallow-water model.

[2]http://envisat.esa.int
[3]http://ilrs.gsfc.nasa.gov/satellite_missions/list_of_satellites/gfo1_general.html

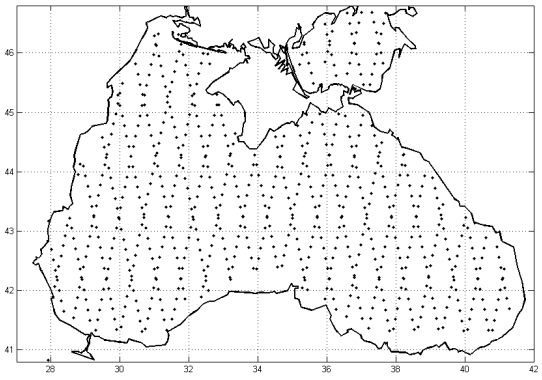

Figure 5: 35 days cycle of Envisat1.

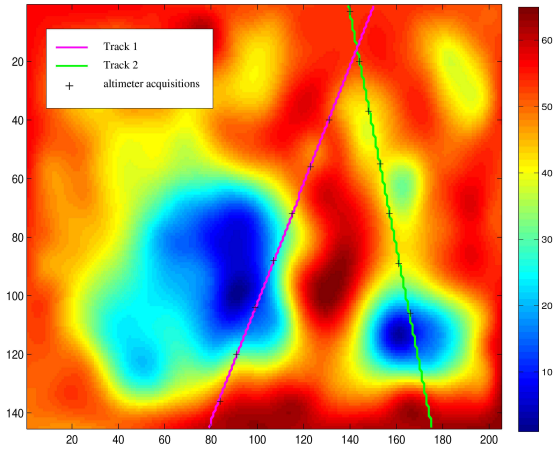

Figure 6: Two altimeter tracks displayed over the average of h_{SWIM}.

Figure 6 displays the value of h_{SWIM}, averaged in time. The two straight lines represent altimeter tracks. The green line comes from Envisat and the pink one from GFO.

The number of altimetry measures available on the same space-time period than the SST data is rather small. However, we apply the conversion given in (19) and perform a quantitative comparison of h_{alt} and h_{SWIM} along a track. Figure 7 displays these curves for the two tracks displayed on Figure 6: on the left with Envisat and on the right with GFO. Black crosses locate the altimeter measures. The shapes and values of h_{alt} and h_{SWIM} curves are very similar.

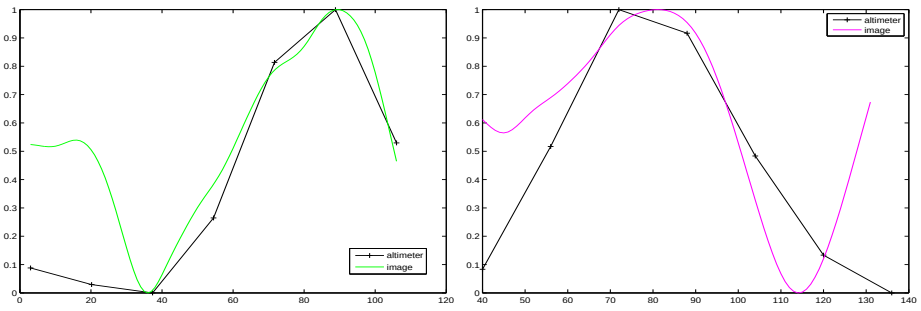

Figure 7: Sea Level Anomaly, given by the altimeters, compared with the estimation with SWIM.

There is no error in the slope directions. The extrema are well localized. It is almost perfect in the case of Envisat. As the velocity field is strongly related to the shape of the thickness image, these promising results on thickness estimation validate the estimation of the motion. Figure 8 illustrates the link between velocity and thickness: a bump correspond to an anticyclonic velocity field and a bowl to a cyclonic one.

6 Conclusion

In this paper, we propose an analysis and validation of the data assimilation approach for motion estimation from satellite image sequences. We compared two dynamic assumptions, *i.e.* we assimilated the same data in two image models, SIM and SWIM, and analyzed motion results. Moreover, we used altimetry data to quantify the quality of the estimation. The comparison between the surface anomaly estimated by SWIM and measured by altimeters validates our approach.

References

[1] B.K.P. Horn and B.G. Schunk, "Determining optical flow," *Artificial Intelligence*, vol. 17, pp. 185–203, 1981.

[2] H.-H. Nagel, "Displacement vectors derived from second-order intensity variations in image sequences," *Computer Vision, Graphics, and Image Processing*, vol. 21, pp. 85–117, 1983.

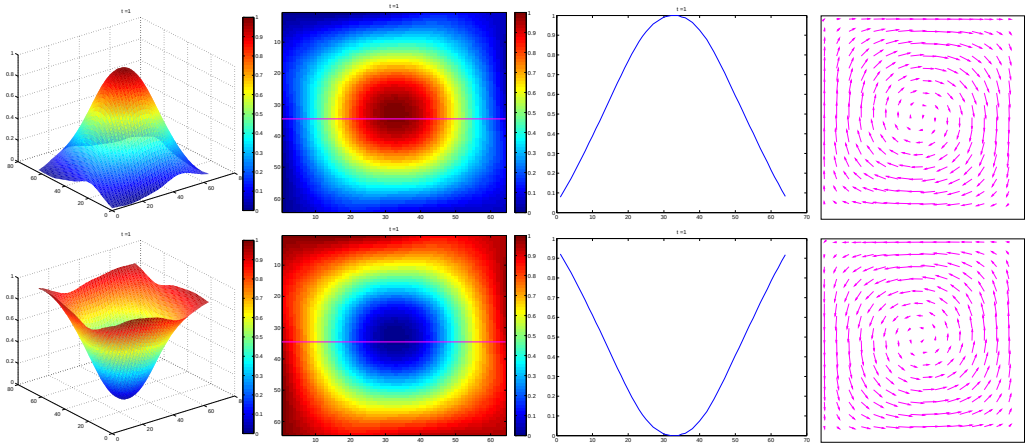

Figure 8: From left to right. 1. 3D water layer thickness. 2. Its 2D projection. The magenta line figures the track of an altimeter. 3. SLA along this track. 4. Velocity field.

[3] I. Cohen and I. Herlin, "Optical flow and phase portrait methods for environmental satellite image sequences," in *Proceedings of European Conference on Computer Vision*, Oxford, UK, April 1996.

[4] E. Mémin and P. Pérez, "Optical flow estimation and object-based segmentation with robust techniques," *IEEE Trans. on Image Processing*, vol. 7, no. 5, pp. 703–719, May 1998.

[5] Dominique Béréziat, Isabelle Herlin, and Laurent Younes, "A generalized optical flow constraint and its physical interpretation," in *CVPR*, 2000, pp. 2487–2492.

[6] T. Corpetti, E. Mémin, and P. Pérez, "Dense estimation of fluid flows," *IEEE Transactions on Pattern Analysis and Machine Intelligence*, vol. 24, no. 3, pp. 365–380, March 2002.

[7] T. Isambert, J.P. Berroir, and I. Herlin, "A multiscale vector spline method for estimating the fluids motion on satellite images," in *Proceedings of European Conference on Computer Vision*, Marseille, France, October 2008, Springer.

[8] I. Herlin, E. Huot, J.-P. Berroir, F.-X. Le Dimet, and G. Korotaev, "Estimation of a motion field on satellite images from a simplified ocean circulation model.," in *Proceedings of International Conference on Image Processing*, Atlanta, USA, October 2006.

[9] N. Papadakis, P. Héas, and É. Mémin, "Image assimilation for motion estimation of atmospheric layers with shallow-water model," in *Proceedings of Asian Conference on Computer Vision*, Tokyo, Japan, November 2007, pp. 864–874.

[10] Dominique Béréziat and Isabelle Herlin, "Solving ill-posed Image Processing problems using Data Assimilation," *Numerical Algorithms*, vol. 56, no. 2, pp. 219–252, February 2011.

[11] O. Titaud, A. Vidard, I. Souopgui, and F.-X. Le Dimet, "Assimilation of image sequences in numerical models," *Tellus A*, vol. 62, pp. 30–47, 2010.

[12] Gennady Korotaev, Etienne Huot, François-Xavier Le Dimet, Isabelle Herlin, Sergey V. Stanichny, Dmitry M. Solovyev, and Lin Wu, "Retrieving ocean surface current by 4-D variational assimilation of sea surface temperature images," *Remote Sensing of Environment*, vol. 112, no. 4, pp. 1464–1475, April 2008, Special issue on data assimilation.

[13] Etienne Huot, Isabelle Herlin, and Gennady Korotaev, "Assimilation of SST Satellite Images for Estimation of Ocean Circulation Velocity," in *Proceedings of IEEE International Geoscience and Remote Sensing Symposium (IGARSS)*, Boston, Massachusetts, U.S.A., July 6-11 2008, vol. 2, pp. 847–850.

[14] Etienne Huot, Isabelle Herlin, Nicolas Mercier, and Evgeny Plotnikov, "Estimating apparent motion on satellite acquisitions with a physical dynamic model," in *Proceedings of the International Conference on Pattern Recognition*, Istanbul, Turkey, August 2010, pp. 41–44, Springer Verlag, MoAT3.1.

Centre de recherche INRIA Paris – Rocquencourt
Domaine de Voluceau - Rocquencourt - BP 105 - 78153 Le Chesnay Cedex (France)

Centre de recherche INRIA Bordeaux – Sud Ouest : Domaine Universitaire - 351, cours de la Libération - 33405 Talence Cedex
Centre de recherche INRIA Grenoble – Rhône-Alpes : 655, avenue de l'Europe - 38334 Montbonnot Saint-Ismier
Centre de recherche INRIA Lille – Nord Europe : Parc Scientifique de la Haute Borne - 40, avenue Halley - 59650 Villeneuve d'Ascq
Centre de recherche INRIA Nancy – Grand Est : LORIA, Technopôle de Nancy-Brabois - Campus scientifique
615, rue du Jardin Botanique - BP 101 - 54602 Villers-lès-Nancy Cedex
Centre de recherche INRIA Rennes – Bretagne Atlantique : IRISA, Campus universitaire de Beaulieu - 35042 Rennes Cedex
Centre de recherche INRIA Saclay – Île-de-France : Parc Orsay Université - ZAC des Vignes : 4, rue Jacques Monod - 91893 Orsay Cedex
Centre de recherche INRIA Sophia Antipolis – Méditerranée : 2004, route des Lucioles - BP 93 - 06902 Sophia Antipolis Cedex

Éditeur
INRIA - Domaine de Voluceau - Rocquencourt, BP 105 - 78153 Le Chesnay Cedex (France)
http://www.inria.fr
ISSN 0249-6399